Comprehensive Electro-Optical Investigation of a Ga-Doped AlN Nanowire LED for Applications in the UV-C Range

Rémy Vermeersch, Eric Robin, Gwénolé Jacopin, Bruno Gayral, Julien Pernot, Bruno Daudin

Comprehensive Electro-Optical Investigation of a Ga-doped AlN Nanowire LED in the UV-C Range

Rémy Vermeersch[1,2,], Eric Robin[3], Gwénolé Jacopin[2], Bruno Gayral[1], Julien Pernot[2], Bruno Daudin[1]*

[1] Univ. Grenoble Alpes, CEA, Grenoble INP, IRIG, PHELIQS, NPSC, 17 rue des martyrs, 38000 Grenoble, France.

[2] Univ. Grenoble Alpes, Grenoble INP, Institut Néel, SC2G, CNRS, 38000 Grenoble, France.

[3] Univ. Grenoble Alpes, CEA, Grenoble INP, IRIG-MEM, LEMMA, 17 rue des martyrs, 38000 Grenoble, France.

Corresponding author: remy.vermeersch@neel.cnrs.fr

Keywords: Nanowire, AlN, LED, UV, electrical transport, doping, exciton.

Abstract:

With the aim of targeting sanitization applications, the realization of a 285 nm AlN nanowire-based light emitting diode is reported, with a focus on the comprehensive study of electro-optical properties. The active region consists of AlGaN, with a Ga content of at most one percent, as measured by energy dispersive X-ray spectroscopy. Optical properties were investigated by means of cathodo- and photoluminescence. They reveal a high degree of localization of electron-hole pairs on recombination centers behaving as quantum dots. The AlN pn-junctions show diode-like rectifying behavior with 5 orders of magnitude difference between +/- 10 V. The main factor limiting the current at larger forward bias is found to be tunnel-limited injection obeying a Fowler-Nordheim model. Spatially resolved cathodoluminescence (CL) and electron-beam induced current measurements demonstrate that the active region overlaps the space charge region. Finally, electroluminescence (EL) spectroscopy was performed. This methodology allowed us to identify current limitations, the main one being injection efficiency, opening the path to efficiency improvement solutions.

Introduction

Solid state ultraviolet (UV) emitters draw an increased interest for a wide variety of applications and particularly for bactericide ones. Compared to the conventional mercury lamps, UV light emitting diodes (LEDs) exhibit numerous advantages such as a low operation voltage, longer lifespan, compactness and absence of harmful mercury. However, despite the demand and research efforts, Al-rich AlGaN thin films LEDs are still lacking efficiency with a record external quantum efficiency (EQE) of 20% at 275 nm[1] but drastically decreasing as the wavelength shortens.[2]

Reasons for this decrease are manifold. As the AlN molar fraction increases, ionization energy of n-type and p-type dopants increases, reducing free charge carrier density and the overall conductivity of the layers.[3–7] In addition, the lack of suitable substrate with low dislocation density,[8] and the difficult extraction of light[9], limit the performances of the device and increase the complexity of the fabrication process.

To address some of those issues, nanowire (NW) based heterostructures are promising. Thanks to their growth mechanism and their geometry, the formation of extended defects is avoided and the extraction of light can be enhanced.[10,11] Moreover, the incorporation of dopants is shown to be eased thanks to nearby free surface allowing elastic strain relaxation.[12–14] However, the growth of controlled AlGaN NWs is difficult as they are prone to alloy fluctuations and spontaneous formation of superlattice-like structure.[15–17] Leveraging those advantages, some groups reported the fabrication of UV LEDs in the UV-B and UV-C range from AlInN[18] and AlGaN NWs,[19] respectively. In spite of these demonstrations, the understanding of electrical transport properties of such AlGaN heterostructures were not discussed or addressed in the scope of giving a picture of the overall properties and performances. This study presents an AlN nanowire-based LED emitting at 285 nm. Contrary to the common quantum well structure, the active area consists of an extremely low Ga-content

AlGaN alloy. The sample exhibits a room temperature / 5 K ratio of integrated cathodoluminescence intensity of ~ 20%, which is assigned to the quantum dot-like behavior of Ga-related carrier localization centers. AlN p-type doping was achieved by Mg/In co-doping,[12] while Si was used for n-type doping.[20,21] The resulting device, presented in the present report, exhibits good electrical properties with a rectifying behavior and high current density. Finally, we used electron beam induced current technique to assess the position of the electric field and check the matching with the active area location. However, it is shown that at high bias, current is limited by tunneling through a potential barrier. Electroluminescence measurements show a single peak at 285 nm, consistent with cathodoluminescence spectrum, and an output optical power scaling linearly with current density. All these characterizations allow one to understand the overall device behavior and unravel the main limitations of the current NW LED design.

The AlN nanowire LED sample was grown by plasma-assisted MBE on highly conductive n-type (111)-Si substrate. The heterostructure consists of a 500 nm long highly conductive n-GaN stem, followed by 150 nm n-type AlN section, a 30 nm Ga-doped AlN active area, a 150 nm long p-type AlN section and a 15 nm p-type GaN cap, measured based on secondary electron contrast from image acquired by scanning electron microscopy (SEM). The AlGaN active area section was grown with an extremely low Ga content of at most 1%, as measured by energy dispersive X-Ray spectroscopy (EDX).[22] This value however does not correspond to the Ga composition of the AlGaN clusters but to an averaged value over the NW diameter. Figure 1 shows a sketch of the sample structure and SEM images from top and cross-sectional view. Enlargement of the nanowires due to the smaller Al adatom diffusion length allowed for the near coalescence of the NW tops, which eased clean room process and contact deposition.

More details on growth parameters and experimental setup can be found in Supporting informationsection A.

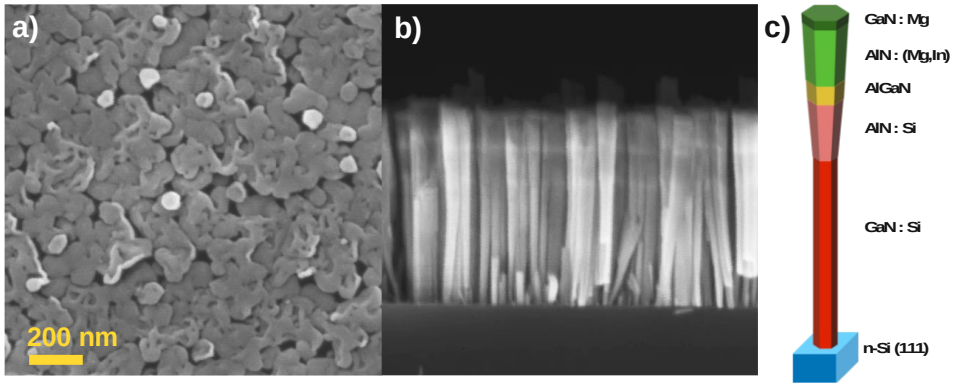

Figure 1: SEM image from top view (a) and cross-sectional view (b) of AlN NW sample. Scale bar stands for both images. (c) Schematic of a single nanowire structure.

The optical properties of the studied sample were first investigated by cathodoluminescence (CL). Figure 2.a. shows a CL spectrum of the sample acquired by scanning a 100 μm^2 area on top of the NWs array, at room temperature, under an acceleration voltage of 15 kV and a probe current of 1.4 nA. The main peak centered at 285 nm is attributed to the signal arising from the active region with contribution from GaN sections at around 360 nm and a blue band at ~ 420 nm. CL spectrum was recorded at various temperatures ranging from 5 K to 315 K (inset of Fig 2.b.) and the integrated signal from the main peak is further plotted as a function of the temperature in Figure 2.b. A marked thermal stability is observed, namely a ratio between the CL signal intensity at 300 K and 5 K of around 20 %. The spectrum in Figure 2.c was obtained by focusing the beam on a single NW, revealing multiple sharp luminescence lines which appear on top of a broader background. Especially, this fine structure in the CL spectra remains present up to around 200 K, as a clue of carrier confinement on recombination centers.

Furthermore, Figure 2.d. shows CL spectra at 5 K for different number of NWs probed. The abundance of emission lines points towards a distribution of strongly confining recombination

centers spanning over a wide energy range. As more and more wires are excited, the overall emission smoothens revealing a random distribution of emission lines centered at ~ 285 nm. In addition, photoluminescence (PL) spectra were acquired under a 244 nm excitation at 5 K and at various powers ranging between 5 to 500 µW, which are shown in Supporting information (Section B). They exhibit no shift either in peak position or normalized intensity pointing towards an absence of saturation of the emission centers, discarding the hypothesis that Donor-Acceptor Pairs (DAP) could be responsible for this luminescence. More details on the optical properties of Ga-rich AlGaN clusters resulting from Ga doping of AlN NWs can be found in ref [22].

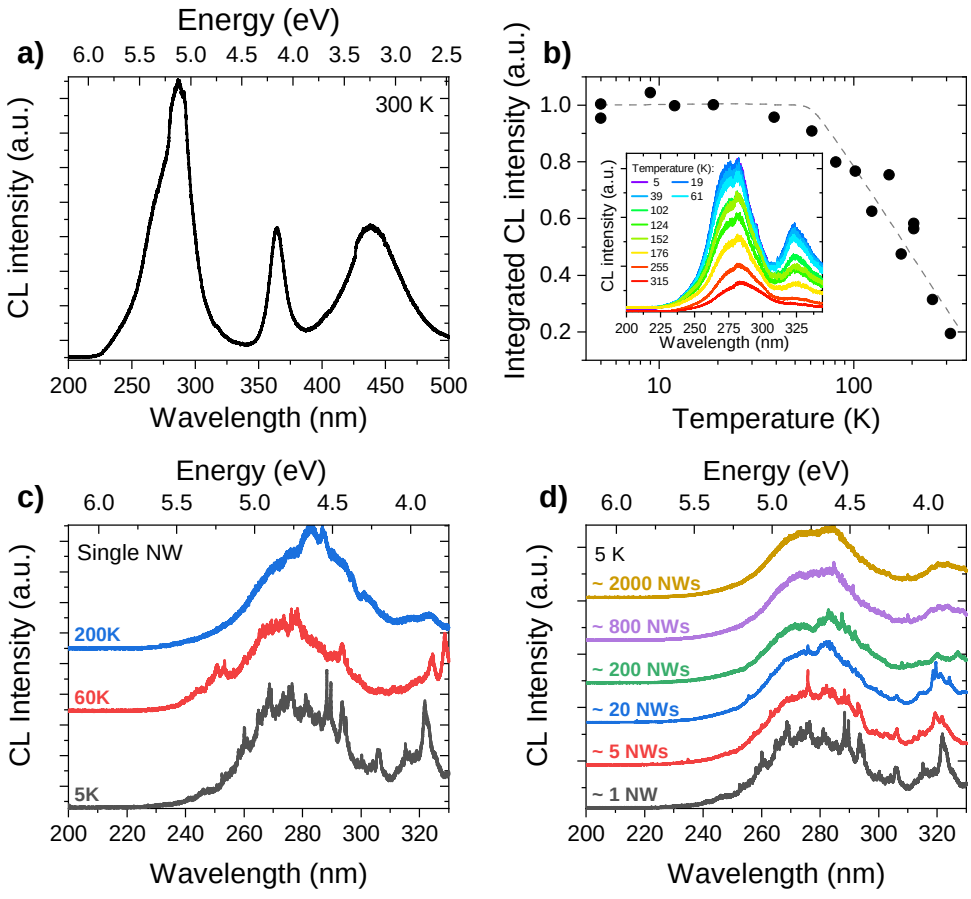

Figure 2: a) Room temperature CL spectrum of the sample taken from the top view on a 100 µm^2 area. b) Integrated CL intensity between 200 nm and 305 nm as function of the temperature and normalized with respect to the average intensity at temperatures lower than 20 K. Dashed

grey line is a guide to the eye. Inset: CL spectrum as function of the temperature. c) CL spectrum with a beam spot focused on a single nanowire acquired at 5 K, 60 K and 200 K. d) CL spectrum at 5 K measured for a number of probed NWs ranging from about 1 to 2000.

J-V characteristics of ten diodes are plotted in a semilogarithmic scale in Figure 3.a. The samples exhibit a rectifying behavior with five orders of magnitude difference between -10 V and +10 V. Good reproducibility from diode to diode is observed up to at least +/- 30 V while keeping the same ON/OFF ratio as shown in Figure 3.b. Several models were considered to account for the transport mechanisms involved in the full structure.

Firstly, at low positive bias, J-V characteristics can be described by the lowering of the pn-junction barrier resulting in thermoionic regime:

$$J = J_{Sat}(\exp\left(\frac{qV}{\eta kT}\right) - 1) \quad (1)$$

with k the Boltzmann constant, T the temperature, q the electron charge, J_{Sat} the saturation current density and η the ideality factor. An ideality factor ~13 can be extracted from the exponential part of the characteristic revealing a non-ideal diode. This huge ideality factor indicates that the thermoionic regime is not the main charge transport mechanism at the pn-junction. Alternately, if one assumes trap assisted tunneling (TAT) at the pn-junction under forward bias, the tunneling current can be defined by[23] :

$$J = A\exp(\frac{qV}{E_T}) \quad (2)$$

Where A is a pre-exponential factor and E_T is a characteristic tunneling energy, found to be equal to 340 meV. TAT is a mechanism in which electrons and holes recombine non-radiatively by tunneling from one band to a defect located in the gap. It is therefore highly detrimental to radiative recombination in LEDs. Its origin may come from the fact that p-AlN section is indeed highly doped with [Mg] ~ 10^{20} cm^{-3} which leads to a short space charge region and ease the

tunnelling of charge carriers. In order to go deeper into this, the tunneling energy can be further expressed as:

$$E_T = \frac{4h}{\pi}\sqrt{\frac{N_I}{m^*\varepsilon_0\varepsilon_r}} \quad (3)$$

with h being the Planck's constant, ε_0 the dielectric permittivity of vacuum, $\varepsilon_r = 9$ the relative dielectric constant of AlN[24], N_I the concentration of impurities and m^* the effective mass of the tunneling particle[23]. The choice of the latter parameter is of importance. By taking into account only electrons with $m_e^* = 0.33$ or only holes with $m_h^* = 4$ [25], N_I takes the values 4 x 10^{16} cm^{-3} or 5 x 10^{17} cm^{-3} respectively. The tunneling occurring in a non-intentionally doped active area, the favored scenario is a tunneling of electrons on residual impurities present at a concentration of 4 x 10^{16} cm^{-3}, in agreement with a previous report[20].

Secondly, at high positive bias, neither ohmic conduction ($J \propto V$) nor space-charge limited current (SCLC) conduction ($J \propto V^2$) is the mechanism limiting the current once the pn-junction is fully lowered. Indeed, this later mechanism occurs when charge carriers are directly injected into the band and has been observed in low conducting AlGaN systems. [20,21,26–28] Instead, J-V measurements fit particularly well to a Fowler-Nordheim (FN) tunneling model, used to describe the emission of charge carriers through a potential barrier. [29,30] In this model, current flow is described by the following equation:

$$J = \frac{qE^2}{16\pi^2\hbar\phi_B}\exp\left(-\frac{4\sqrt{2m^*}(q\phi_B)^{\frac{3}{2}}}{3\hbar q\varepsilon_r E}\right) \quad (4)$$

where E is the electric field and ϕ_B the barrier height. Then, by plotting the quantity $\ln(J/E^2)$ with respect to 1/E, one can obtain a so-called FN plot. By assuming that the potential is fully applied on a triangular shaped barrier, FN plot can be equivalently plotted as $\ln(J/V^2)$ vs 1/V.

Figure 3.c. shows J-V characteristics of the sample in a FN plot for different temperatures between 6 K and 300 K. The linear part at bias higher than ~ 5 V clearly indicates that the current follows this model and that current is limited by either electrons or holes having to

tunnel through a barrier in order to reach their respective bands. As the temperature decreases, one can clearly observe the disappearance of the TAT regime, consistent with the freezing of carriers in the pn-junction.

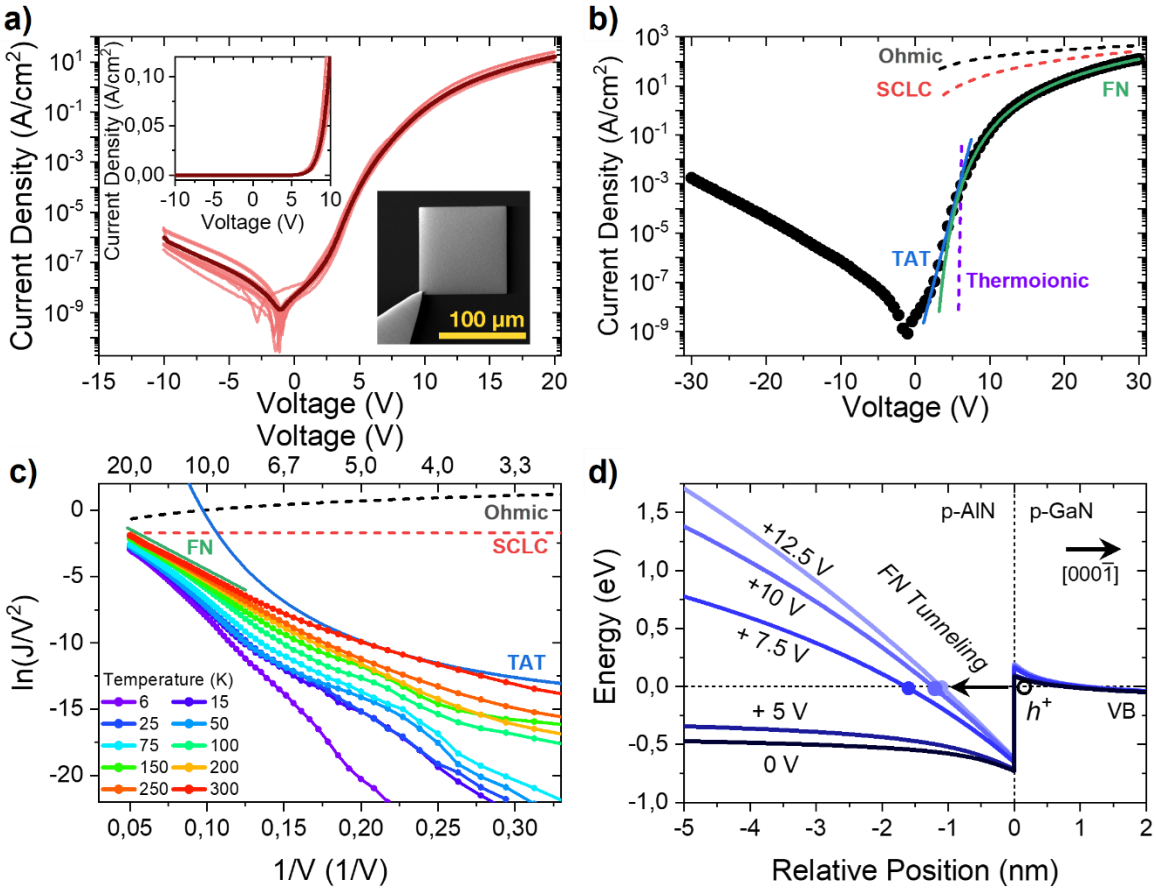

Figure 3: (a) Room temperature Current-voltage (J-V) characteristics of ten AlN NWs LEDs. Dark red curve is the averaged curve. Upper left inset: J-V characteristics in a lin-lin scale. Lower right inset: SE image of a contacted device. (b) Room temperature J-V characteristics of one diode between -30 V and +30 V (open circles) with fits of trap-assisted tunneling (TAT) ($J \propto \exp(V)$), Fowler-Nordheim (FN) ($J \propto V^2 \exp(1/V)$) (straight lines). The expected dependences according to ohmic ($J \propto V$), space charge limited current (SCLC) ($J \propto V^2$) and thermoionic ($J \propto \exp\left(\frac{V}{kT}\right)$) models are also shown, represented with dashed lines. Detection limit is of 10^{-9} A/cm^2. (c) Fowler-Nordheim (FN) plot of the J-V characteristics as function of temperature. Lines represent FN (solid green), TAT (solid blue), ohmic (dash-dot) and SCLC

(dashes) conduction models. (d) Simulated valence band for bias between 0 V and 12.5 V, zoomed at the p-AlN / p-GaN interface. Energies have been normalized with respect to the simulated hole Fermi level at the p-contact.

The origin of this barrier is still unclear. However, since the n-GaN stem is doped up to a metallic level[14] and no FN tunneling has been observed in n-GaN – n-AlN – n-GaN system previously studied,[20] the remaining interfaces are either the pn-junction, the p-AlN / p-GaN interface or the p-GaN / metal interface. Changing Pt/Pd/Au metal stack for a Ni/Au one had no conclusive effect on the high voltage regime, therefore one can assume that this latter interface is not at the origin of the FN tunneling which limits the current. With a valence band offset between AlN and GaN of around 1 eV[31–33], in addition to the reduced hole concentrations in p-section, the p-AlN / p-GaN interface is the most designated candidate to account for this barrier. This hypothesis is further supported by *NextNano* simulations as shown in Figure 3.d, which illustrates the evolution of valence band at the p-AlN / p-GaN interface under different applied bias. It confirms the shape of the valence band, allowing tunneling through this barrier which lowers as the bias increases. The identification of this bottleneck is an additional argument for the replacement of the UV-absorbing p-GaN contact layer by a UV-transparent hole injector such as h-BN[34], graphene[35] or diamond.[36]

Surprisingly, current is flowing even at temperature as low as 6 K at which all carriers should be frozen in regard of the ionization energies of shallowest Si donor state of 75 meV[20] and Mg of ~550 meV[37] in AlN. To explain this feature, a scenario involving direct injection of carriers into their respective bands is put forward. On the one hand, holes can be provided to AlN VB by FN tunneling from p-GaN section. Especially, Figure 3.d. shows that holes are accumulating at the p-GaN / p-AlN interface. Direct injection of holes in p-GaN from the contact by SCLC

is also plausible especially due to the reduced size of the p-GaN layer of only 15 - 20 nm. SCLC scaling with the cube of the layer thickness[38], a high current can be injected at a low bias. On the other hand, electrons are provided by the metallic n-GaN stem and are directly injected into the n-AlN CB by SCLC as reported in a previous study[20]. Once injected in the bands, the electric field is enough to make both charge carriers drift to the active region.

In order to perform further characterizations, the sample was cleaved to access the NWs array from the side. In this configuration, electron-beam induced current (EBIC) at 0 V and CL signals were recorded under a 5 keV electron beam excitation. Since EBIC implies the collection of injected charges, their separation by the internal electric field results in the absence of recombination in this area and would concomitantly result in the absence of CL signal. To cope with this issue CL was acquired on contact-free NWs in the vicinity of the contacted ones used for EBIC measurements. Zero bias EBIC and CL linescans are displayed in Figure 4.a. and b. From the EBIC signal, the pn-junction can clearly be located at the middle of the AlN section, with the electric field reaching a plateau corresponding to the space charge region with a width of around 100 nm. In the case of an abrupt pn-junction, this width *w* is expressed as:

$$w = \sqrt{\frac{2\varepsilon(V_{bi}-V)}{qN_{eff}}} \quad (5)$$

with $N_{eff} = \left(\frac{1}{N_D} + \frac{1}{N_A}\right)^{-1}$, $N_{D,A}$ the donor and acceptor concentrations and V_{bi} the built-in voltage taken as equal to 5.5 V, to account for ionization energy of dopants. With a depletion width of 100 nm, the equivalent N_{eff} is 5 x 10^{17} cm^{-3}. This result gives a lower limit for the dopant concentration, assigned to the n-type one and assesses a significant effective p-type doping of the AlN section.

Away from the depletion region, EBIC signal scales with $e^{-\frac{x}{L_{n,p}}}$ where $L_{n,p}$ is the minority carrier diffusion length. Accordingly, fits were performed and are plotted as black

dashed lines on Figure 4.a. Diffusion lengths of ~ 80 ± 10 nm for electrons in p-AlN and ~ 205 ± 15 nm for holes in n-AlN are found which are close to the ones found in other AlGaN systems[26,39,40]. Furthermore, a shift of the EBIC signal at the top of the wire at the p-AlN / p-GaN section is measured, revealing the tunnel barrier previously mentioned. CL linescan centered on 285 nm shows a maximum intensity aligned with the maximum of EBIC signal. In addition, Figure 4.c. and d. show signals acquired as the electron beam was scanning the sample. It highlights the good homogeneity from wires to wires of both CL and EBIC signals. EBIC and CL correlation is favorable to the injection of charge carriers in the active area in order to make them recombine as efficiently as possible and emit photons at the desired wavelength.

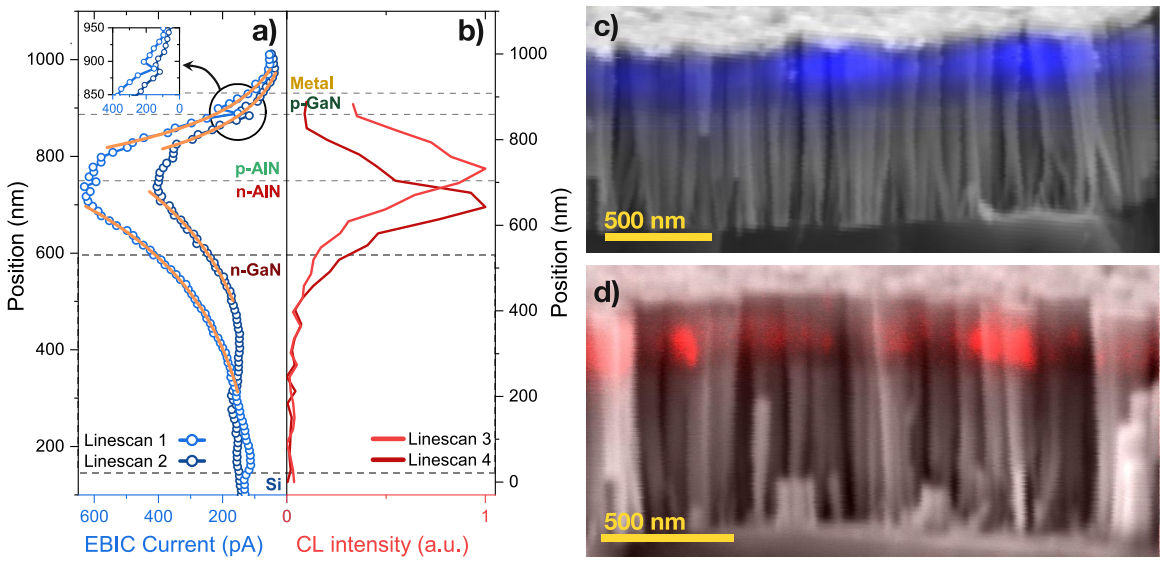

Figure 4: (a) Quantitative EBIC signal at zero bias in blue along with exponential fits in orange solid lines and (b) CL signal recorded along four NWs. Inset in (a) is a zoom showing the EBIC shift at the p-AlN / p-GAN interface. (c) Zero bias EBIC mapping. (d) CL mapping at 285 nm ± 3 nm.

Electroluminescence of the LED was recorded by applying a DC voltage on circular pads displayed on Figure 5.a. in order to collect light from the top. Figure 5.b. shows electroluminescence spectra as a function of the applied bias. One single peak at 285 nm can be seen, which increases with voltage and current. Furthermore, the onset of the EL signal starting at 6 V (inset of Figure 5.b) is consistent with the bandgap of AlN and the LED band structure (see Supporting informationsection C). CL spectrum acquired from top view with a 15 kV acceleration voltage on a 10 x 10 μm^2 region at the center of the pad, and EL spectrum at + 20 V are compared on Figure 5.c. Besides a good agreement of the main peak wavelength position, no significant contribution of GaN or defect related luminescence at higher wavelength is present in EL with respect to CL. This feature points toward recombination of carriers mainly in the active area, even at bias as high as 20 V. To go one step further, EL intensities were integrated, divided by the current density and plotted as function of the current density on Figure 5.d. This plot allows one to identify a plateau for current density lower than 0.2 A/cm^2 meaning that optical power scales linearly with the current density. This is typically expected for LEDs as the optical power is the product of current density and external quantum efficiency. At injection higher than 0.2 A/cm^2, a drop is measured indicating the apparition of losses.

The device efficiency was measured using another top pad design, different from the one in Figure 5.a. It consisted of a 15 nm thick Pt/Pd/Au top metallic layer acting as a semi-transparent electrode. This new pad design and the corresponding EL spectrum are shown in Figures S6 and S7 of the Supporting information. The absorption of this layer is estimated to 40 % from CL measurements. The resulting increase in light collection compared to the ring-shaped pad is however accompanied by a reduction of current density by a factor of 10 due to higher contact resistance. Despite this, optical power could be measured using a power-meter facing the sample top surface. Wall plug efficiency (WPE) and external quantum efficiency

(EQE) of around $2x10^{-3}$ % and $5x10^{-3}$ % are measured. Limitations are attributed to a rather low injection efficiency due to TAT non-radiative recombination and hole injection limited by FN tunneling.

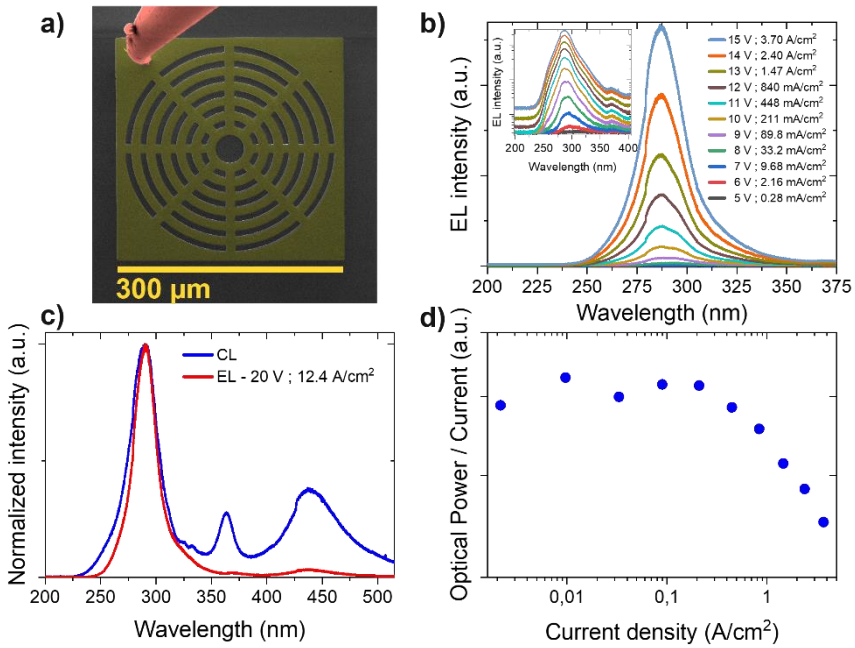

Figure 5: (a) SE image of the contacted pad. Red: tungsten tip. Yellow: metal pad. (b) Electroluminescence spectra peaking at 285 nm. Inset: same data plotted in a logarithmic scale. (c) Comparison between normalized electroluminescence and cathodoluminescence spectra. (d) Ratio of optical power over current density as a function of current density.

Conclusion

To summarize, the realization of an AlN LED emitting at 285 nm grown by MBE was achieved and a methodology was developed in order to investigate its properties and limitations. Optical and structural characterization of the emitting region point toward an original system in which a small amount of Ga is unevenly distributed in AlN. This situation differs from standard short-range composition fluctuations in the Ga content of AlGaN quantum wells, which results in quantum dot (QD)-like behavior and strong exciton localization. Although, the nature of localization centers in Ga-doped AlN is basically different, the random distribution of Ga atoms in the AlN matrix is leading to a similar QD-like behavior at the scale probed by

the AlN exciton. The pn-junction shows good reproducibility and performances although limited by the presence of a tunnel barrier assumed to be at the p-AlN / p-GaN interface. By modeling of I-V and EBIC, a high effective n-type doping of 5 x 10^{17} cm^{-3} was extracted as well as diffusion lengths of around 80 nm and 200 nm for electrons and holes in p-AlN and n-AlN respectively. Electroluminescence was successfully obtained, consistent with optical measurements. Devices behavior is in line with standard LEDs and an EQE of around 2 x 10^{-3} % is measured. Using several characterization techniques specific to such nanoscale devices, injection efficiency is identified as the main limiting factor because of TAT mechanisms favored by the large acceptor concentration in the p-AlN section. Further development will rely on the improvement of the pn-junction electrostatics and investigation of better top contact to replace p-GaN. This work provides a route for understanding limitations and bottlenecks of nanowire optoelectronic device to further improve their design and performances.

Supporting Information

Experimental details of the sample's growth, TEM and EDX measurements, CL and PL measurements, clean room process and electrical characterization. Power-dependent PL measurement of the sample. NextNano simulation of the band structure under various applied bias and mobility. Details on the optical power measurement.

Acknowledgments

The authors thank Y. Genuist, Y. Curé and F. Jourdan for technical support during MBE growth, Dr. F. Donatini for his help with the CL and EBIC setup and the Nanofab team for the use of their facilities and technical assistance. We acknowledge support from GANEXT (ANR-11-LABX-0014) . GANEXT belongs to the public funded 'Investissements d' Avenir' program managed by the French ANR agency.

The authors declare no conflict of interests.

References

(1) Takano, T.; Mino, T.; Sakai, J.; Noguchi, N.; Tsubaki, K.; Hirayama, H. Deep-Ultraviolet Light-Emitting Diodes with External Quantum Efficiency Higher than 20% at 275 Nm Achieved by Improving Light-Extraction Efficiency. *Appl. Phys. Express* **2017**, *10* (3). https://doi.org/10.7567/APEX.10.031002.

(2) Amano, H.; Collazo, R.; Santi, C. De; Einfeldt, S.; Funato, M.; Glaab, J.; Hagedorn, S.; Hirano, A.; Hirayama, H.; Ishii, R.; Kashima, Y.; Kawakami, Y.; Kirste, R.; Kneissl, M.; Martin, R.; Mehnke, F.; Meneghini, M.; Ougazzaden, A.; Parbrook, P. J.; Rajan, S.; Reddy, P.; Römer, F.; Ruschel, J.; Sarkar, B.; Scholz, F.; Schowalter, L. J.; Shields, P.; Sitar, Z.; Sulmoni, L.; Wang, T.; Wernicke, T.; Weyers, M.; Witzigmann, B.; Wu, Y.-R.; Wunderer, T.; Zhang, Y. The 2020 UV Emitter Roadmap. *J. Phys. D. Appl. Phys.* **2020**, *53* (50), 503001. https://doi.org/10.1088/1361-6463/aba64c.

(3) Pampili, P.; Parbrook, P. J. Doping of III-Nitride Materials. *Mater. Sci. Semicond. Process.* **2017**, *62* (October), 180–191. https://doi.org/10.1016/j.mssp.2016.11.006.

(4) Nakarmi, M. L.; Kim, K. H.; Zhu, K.; Lin, J. Y.; Jiang, H. X. Transport Properties of Highly Conductive N-Type Al-Rich AlxGa1−xN(X⩾0.7). *Appl. Phys. Lett.* **2004**, *85* (17), 3769–3771. https://doi.org/10.1063/1.1809272.

(5) Mireles, F.; Ulloa, S. E. Acceptor Binding Energies in GaN and AlN. *Mater. Res. Soc. Symp. - Proc.* **1997**, *482* (7), 839–844. https://doi.org/10.1557/proc-482-839.

(6) Taniyasu, Y.; Kasu, M.; Makimoto, T. An Aluminium Nitride Light-Emitting Diode with a Wavelength of 210 Nanometres. *Nature* **2006**, *441* (7091), 325–328. https://doi.org/10.1038/nature04760.

(7) Mehnke, F.; Trinh, X. T.; Pingel, H.; Wernicke, T.; Janzén, E.; Son, N. T.; Kneissl, M.

Electronic Properties of Si-Doped Alx Ga 1 - X N with Aluminum Mole Fractions above 80%. *J. Appl. Phys.* **2016**, *120* (14). https://doi.org/10.1063/1.4964442.

(8) Ban, K.; Yamamoto, J. I.; Takeda, K.; Ide, K.; Iwaya, M.; Takeuchi, T.; Kamiyama, S.; Akasaki, I.; Amano, H. Internal Quantum Efficiency of Whole-Composition-Range AlGaN Multiquantum Wells. *Appl. Phys. Express* **2011**, *4* (5), 52101. https://doi.org/10.1143/apex.4.052101.

(9) Guttmann, M.; Mehnke, F.; Belde, B.; Wolf, F.; Reich, C.; Sulmoni, L.; Wernicke, T.; Kneissl, M. Optical Light Polarization and Light Extraction Efficiency of AlGaN-Based LEDs Emitting between 264 and 220 Nm. *Jpn. J. Appl. Phys.* **2019**, *58* (SC). https://doi.org/10.7567/1347-4065/ab0d09.

(10) Wei, T.; Islam, S. M.; Jahn, U.; Yan, J.; Lee, K.; Bharadwaj, S.; Ji, X.; Wang, J.; Li, J.; Protasenko, V.; Xing, H. (Grace); Jena, D. GaN/AlN Quantum-Disk Nanorod 280 Nm Deep Ultraviolet Light Emitting Diodes by Molecular Beam Epitaxy. *Opt. Lett.* **2020**, *45* (1), 121. https://doi.org/10.1364/OL.45.000121.

(11) Djavid, M.; Mi, Z. Enhancing the Light Extraction Efficiency of AlGaN Deep Ultraviolet Light Emitting Diodes by Using Nanowire Structures. *Appl. Phys. Lett.* **2016**, *108* (5). https://doi.org/10.1063/1.4941239.

(12) Siladie, A.-M.; Jacopin, G.; Cros, A.; Garro, N.; Robin, E.; Caliste, D.; Pochet, P.; Donatini, F.; Pernot, J.; Daudin, B. Mg and In Codoped P-Type AlN Nanowires for Pn Junction Realization. *Nano Lett.* **2019**, *19* (12), 8357–8364. https://doi.org/10.1021/acs.nanolett.9b01394.

(13) Tang, Y. B.; Bo, X. H.; Xu, J.; Cao, Y. L.; Chen, Z. H.; Song, H. S.; Liu, C. P.; Hung, T. F.; Zhang, W. J.; Cheng, H. M.; Bello, I.; Lee, S. T.; Lee, C. S. Tunable P-Type

Conductivity and Transport Properties of AlN Nanowires via Mg Doping. *ACS Nano* **2011**, *5* (5), 3591–3598. https://doi.org/10.1021/nn200963k.

(14) Fang, Z.; Robin, E.; Rozas-Jiménez, E.; Cros, A.; Donatini, F.; Mollard, N.; Pernot, J.; Daudin, B. Si Donor Incorporation in GaN Nanowires. *Nano Lett.* **2015**, *15* (10), 6794–6801. https://doi.org/10.1021/acs.nanolett.5b02634.

(15) Belloeil, M.; Gayral, B.; Daudin, B. Quantum Dot-Like Behavior of Compositional Fluctuations in AlGaN Nanowires. *Nano Lett.* **2016**, *16* (2), 960–966. https://doi.org/10.1021/acs.nanolett.5b03904.

(16) Belloeil, M.; Proietti, M. G.; Renevier, H.; Daudin, B. Nanoscale X-Ray Investigation of Composition Fluctuations in AlGaN Nanowires. *Nanotechnology* **2020**, *31* (37). https://doi.org/10.1088/1361-6528/ab94e1.

(17) Pierret, A.; Bougerol, C.; Gayral, B.; Kociak, M.; Daudin, B. Probing Alloy Composition Gradient and Nanometer-Scale Carrier Localization in Single AlGaN Nanowires by Nanocathodoluminescence. *Nanotechnology* **2013**, *24* (30). https://doi.org/10.1088/0957-4484/24/30/305703.

(18) Velpula, R. T.; Jain, B.; Philip, M. R.; Nguyen, H. D.; Wang, R.; Nguyen, H. P. T. Epitaxial Growth and Characterization of AlInN-Based Core-Shell Nanowire Light Emitting Diodes Operating in the Ultraviolet Spectrum. *Sci. Rep.* **2020**, *10* (1), 1–10. https://doi.org/10.1038/s41598-020-59442-0.

(19) Zhao, S.; Connie, A. T.; Dastjerdi, M. H. T.; Kong, X. H.; Wang, Q.; Djavid, M.; Sadaf, S.; Liu, X. D.; Shih, I.; Guo, H.; Mi, Z. Aluminum Nitride Nanowire Light Emitting Diodes: Breaking the Fundamental Bottleneck of Deep Ultraviolet Light Sources. *Sci. Rep.* **2014**, *5*, 1–5. https://doi.org/10.1038/srep08332.

(20) Vermeersch, R.; Robin, E.; Cros, A.; Jacopin, G.; Daudin, B.; Pernot, J. Shallow Donor and DX State in Si Doped AlN Nanowires Grown by Molecular Beam Epitaxy. *Appl. Phys. Lett.* **2021**, *119* (26). https://doi.org/10.1063/5.0074454.

(21) Vermeersch, R.; Jacopin, G.; Daudin, B.; Pernot, J. DX Center Formation in Highly Si Doped AlN Nanowires Revealed by Trap Assisted Space-Charge Limited Current. *Appl. Phys. Lett.* **2022**, *120* (16). https://doi.org/10.1063/5.0087789.

(22) Vermeersch, R.; Jacopin, G.; Robin, E.; Pernot, J.; Gayral, B.; Daudin, B. Optical Properties of Ga-Doped AlN Nanowires. *Appl. Phys. Lett.* **2023**, *122* (9). https://doi.org/10.1063/5.0137424.

(23) Lee, K. B.; Parbrook, P. J.; Wang, T.; Bai, J.; Ranalli, F.; Airey, R. J.; Hill, G. The Origin of the High Ideality Factor in AlGaN-Based Quantum Well Ultraviolet Light Emitting Diodes. *Phys. Status Solidi Basic Res.* **2010**, *247* (7), 1761–1763. https://doi.org/10.1002/pssb.200983617.

(24) Thorp, J. S.; Evans, D.; Al-Naief, M.; Akhtaruzzaman, M. The Dielectric Properties of Aluminium Nitride Substrates for Microelectronics Packaging. *J. Mater. Sci.* **1990**, *25* (12), 4965–4971. https://doi.org/10.1007/BF00580114.

(25) Rinke, P.; Winkelnkemper, M.; Qteish, A.; Bimberg, D.; Neugebauer, J.; Scheffler, M. Consistent Set of Band Parameters for the Group-III Nitrides AlN, GaN, and InN. *Phys. Rev. B - Condens. Matter Mater. Phys.* **2008**, *77* (7), 1–15. https://doi.org/10.1103/PhysRevB.77.075202.

(26) Fang, Z.; Donatini, F.; Daudin, B.; Pernot, J. Axial p–n Junction and Space Charge Limited Current in Single GaN Nanowire. *Nanotechnology* **2018**, *29* (1), 01LT01. https://doi.org/10/ggbhf7.

(27) Vesely, J. C.; Shatzkes, M.; Burkhardt, P. J. Space-Charge-Limited Current Flow in Gallium Nitride Thin Films. *Phys. Rev. B* **1974**, *10* (2), 582–590. https://doi.org/10.1103/PhysRevB.10.582.

(28) Lebedev, V.; Cherkashinin, G.; Ecke, G.; Cimalla, I.; Ambacher, O. Space Charge Limited Electron Transport in AlGaN Photoconductors. *J. Appl. Phys.* **2007**, *101* (3). https://doi.org/10.1063/1.2433139.

(29) Lenzlinger, M.; Snow, E. H. Fowler-Nordheim Tunneling into Thermally Grown SiO2. *J. Appl. Phys.* **1969**, *40* (1), 278–283. https://doi.org/10.1063/1.1657043.

(30) Karasawa, A.; Makino, T.; Traore, A.; Kato, H.; Ogura, M.; Kato, Y.; Takeuchi, D.; Yamasaki, S.; Sakurai, T. Carrier Transport Mechanism of Diamond P+-n Junction at Low Temperature Using Schottky-Pn Junction Structure. *Jpn. J. Appl. Phys.* **2021**, *60* (3). https://doi.org/10.35848/1347-4065/abe33f.

(31) Neugebauer, C. G. V. D. W.; Walle, C. G. Van De. Small Valence-Band Offsets at GaN / InGaN Heterojunctions Small Valence-Band Offsets at GaN / InGaN Heterojunctions. **2009**, *2577* (1997), 10–13.

(32) Satpathy, S.; Popovic, Z. S.; Mitchel, W. C. Theory of the Composition Dependence of the Band Offset and Sheet Carrier Density in the GaN/AlxGa1-XN Heterestructure. *J. Appl. Phys.* **2004**, *95* (10), 5597–5601. https://doi.org/10.1063/1.1704869.

(33) Martin, G.; Botchkarev, A.; Rockett, A.; Morkoç, H. Valence-Band Discontinuities of Wurtzite GaN, AlN, and InN Heterojunctions Measured by x-Ray Photoemission Spectroscopy. *Appl. Phys. Lett.* **1995**, No. April 1996, 2541. https://doi.org/10.1063/1.116177.

(34) Laleyan, D. A.; Zhao, S.; Woo, S. Y.; Tran, H. N.; Le, H. B.; Szkopek, T.; Guo, H.;

Botton, G. A.; Mi, Z. AlN/h-BN Heterostructures for Mg Dopant-Free Deep Ultraviolet Photonics. *Nano Lett.* **2017**, *17* (6), 3738–3743. https://doi.org/10.1021/acs.nanolett.7b01068.

(35) Kim, B. J.; Lee, C.; Jung, Y.; Hyeon Baik, K.; Mastro, M. A.; Hite, J. K.; Eddy, C. R.; Kim, J. Large-Area Transparent Conductive Few-Layer Graphene Electrode in GaN-Based Ultra-Violet Light-Emitting Diodes. *Appl. Phys. Lett.* **2011**, *99* (14), 1–4. https://doi.org/10.1063/1.3644496.

(36) SILADIE, A.-M.; Daudin, B.; JACOPIN, G.; Pernot, J. Light-Emitting Diode Comprising a Semiconductor Based on Aln p-Doped with Atoms of Magnesium and a Layer of Doped Diamond. W O 2021/074519 A1, 2020.

(37) Nam, K. B.; Nakarmi, M. L.; Li, J.; Lin, J. Y.; Jiang, H. X. Mg Acceptor Level in AlN Probed by Deep Ultraviolet Photoluminescence. *Appl. Phys. Lett.* **2003**, *83* (5), 878–880. https://doi.org/10.1063/1.1594833.

(38) Lampert, M. A. Simplified Theory of Space-Charge-Limited Currents in an Insulator with Traps. *Phys. Rev.* **1956**, *103* (6), 1648–1656. https://doi.org/10.1103/PhysRev.103.1648.

(39) Piazza, V.; Babichev, A. V.; Mancini, L.; Morassi, M.; Quach, P.; Bayle, F.; Largeau, L.; Julien, F. H.; Rale, P.; Collin, S.; Harmand, J.-C. C.; Gogneau, N.; Tchernycheva, M. Investigation of GaN Nanowires Containing AlN/GaN Multiple Quantum Discs by EBIC and CL Techniques. *Nanotechnology* **2019**, *30* (21), 214006. https://doi.org/10/gf98v7.

(40) Chernyak, L.; Osinsky, A.; Fuflyigin, V.; Schubert, E. F. Electron Beam-Induced Increase of Electron Diffusion Length in p-Type GaN and AlGaN/GaN Superlattices.

Appl. Phys. Lett. **2000**, *77* (6), 875–877. https://doi.org/10.1063/1.1306910.